Eur. Radiol. 9, 16–28 (1999)

European
Radiology

Pictorial review

CT and MRI of the male genital tract: radiologic–pathologic correlation

R. A. Kubik-Huch[1], **S. Hailemariam**[2], **B. Hamm**[3]

[1] Department of Radiology, University Hospital, Rämistrasse 100, CH-8091 Zurich, Switzerland
[2] Department of Pathology, University Hospital, Rämistrasse 100, CH-8091 Zurich, Switzerland
[3] Department of Radiology, Hospital Charité, Berlin, Germany

Received 28 May 1998; Revision received 13 July 1998; Accepted 17 July 1998

Abstract. Technical advances in magnetic resonance imaging (MRI), notably in high-resolution MRI, have opened up new diagnostic applications in male pelvic pathology. A major indication is the preoperative staging of prostate cancer, where MRI is more reliable than other imaging modalities in differentiating between localized and advanced disease. In monitoring local recurrence after radical prostatectomy MRI is also valuable in differentiating scar tissue from new growth. In benign prostate disease, MRI effectively displays the congenital cysts that may be associated with infertility. Other disease, however – notably benign prostatic hyperplasia – is generally an incidental finding. Ultrasound remains the imaging modality of choice for evaluation of pathologies of the penis, testis and scrotum, e. g. in differentiating malignant from benign scrotal masses or in diagnosing acute scrotum due to testicular torsion or rupture. In isolated cases, MRI is also a valuable diagnostic aid in conditions of these organs, e. g. in the preoperative localization of ectopic testes in cryptorchidism or if US findings are equivocal.

Key words: CT, MRI, prostate, testis

Introduction

Technical advances in computed tomography (CT) and magnetic resonance imaging (MRI) have opened up new diagnostic applications in male pelvic pathology. Cross-sectional imaging modalities thus play an increasing role in the diagnosis, staging, and follow-up of a variety of diseases of the male pelvis.

Ultrasound (US), nowadays often considered an extension of the physical examination, is the imaging modality of choice for initial assessment of a pathologic condition. In many cases, it supplies sufficient information to establish the correct diagnosis. CT and MRI are indicated in all cases in which US findings are equivocal or a discrepancy between clinical and sonographic findings exists. A major indication for MRI is, furthermore, the preoperative local tumor staging of prostate cancer. In addition, CT and MRI are important tools for staging of malignant disease, e. g. in testicular cancer.

This review article attempts to give an overview of the potential and limitations of these imaging modalities in diagnosing and staging disorders of the male genital organs, with special emphasis on radiologic-pathologic correlation.

Correspondence to: R. A. Kubik-Huch

The prostate

High spatial resolution and high soft tissue contrast are prerequisites for any imaging modality aimed at the centimeter-wide target of prostate and seminal vesicles. Magnetic resonance imaging (MRI) is superior to computed tomography (CT) in this regard and supplements urologic transrectal US, particularly if an endorectal surface coil is combined with a pelvic phased-array coil [1].

Normal anatomy

The three anatomic zones of the prostate comprise a posterolateral peripheral zone (accounting for most of the gland's volume), a central zone (approximately 25 %) forming the bulk of the prostate base, and a transition zone enclosing the prostatic urethra and accounting for approximately 5–10 % of the volume in the young adult. The latter zone is the tissue responsible for the benign prostate hyperplasia (BPH) which in the elderly compromises the other structures and urinary function [2].

On MRI the prostate is hypointense and homogeneous on T1-weighted images. The different zones can be identified only on T2-weighted images, which show

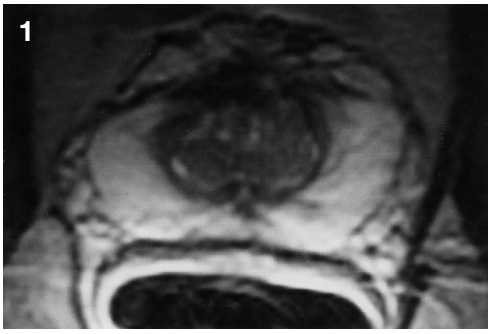

Fig. 1. Normal prostate gland. Axial endorectal T2-weighted fast spin-echo (FSE) image. The hyperintense peripheral zone can be distinguished from the hypointense central gland

Fig. 2 A–C. Normal seminal vesicles. **A, B** MRI: The content of seminal vesicles presents hyperintense on the axial endorectal T2-weighted FSE image **(A)** and hypointense on the contrast-enhanced T1-weighted image **(B)**, and the septa show avid contrast enhancement. The midline structure of intermediate signal intensity on both sequences represents the ductus deferens. **C** Hematoxylin and eosin stain (magnification × 35): normal seminal vesicles

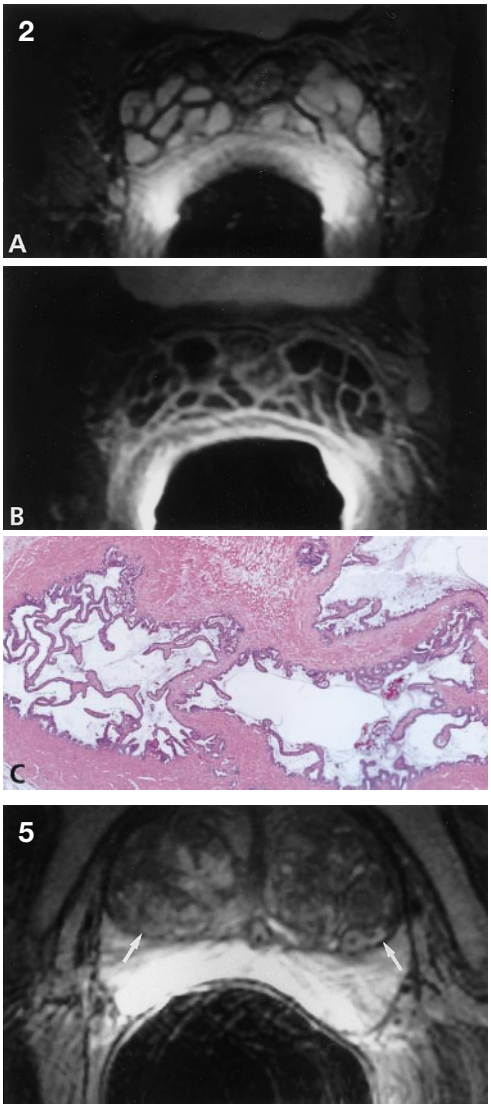

Fig. 5. Axial endorectal T2-weighted FSE image in a patient with benign prostatic hyperplasia. Enlarged transitional zone of inhomogeneous medium signal intensity *(arrows)*. Normal hyperintense peripheral zone

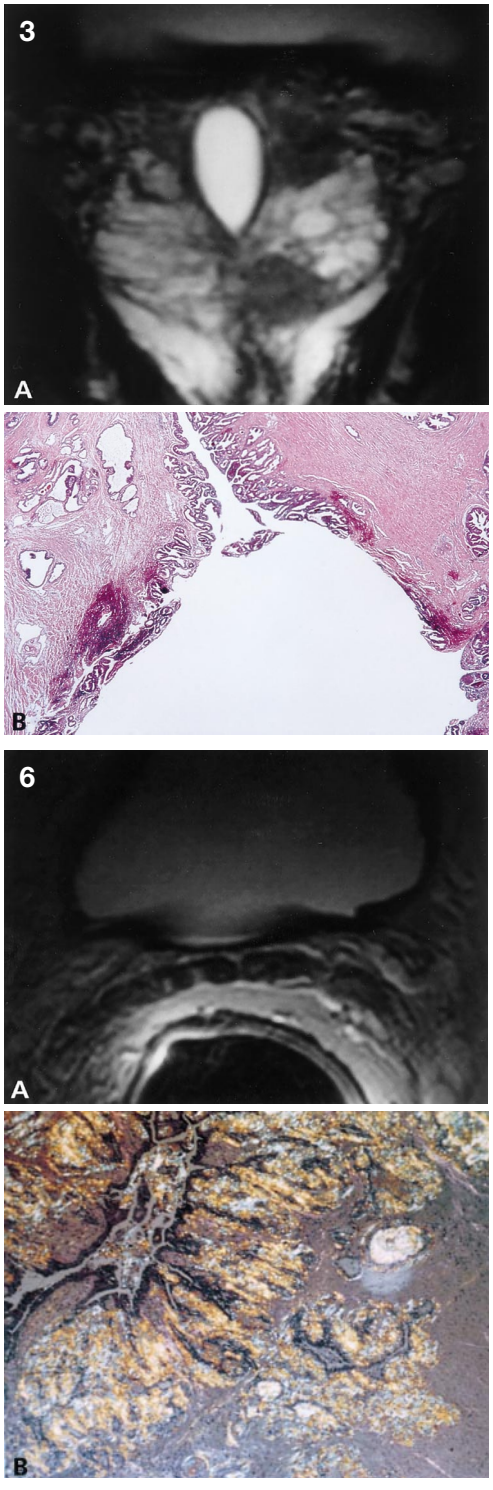

Fig. 3 A, B. Incidental diagnosis of congenital prostate cyst in a 58-year-old patient with multifocal stage T2 prostate carcinoma. **A** Coronal endorectal T2-weighted FSE image. The normally hyperintense peripheral zone contains two hypointense foci on the left side compatible with infiltrating carcinoma. **B** Hematoxylin and eosin stain (magnification × 25): The hyperintense midline cyst seen on MRI is consistent with cystic dilatation of the utriculus

Fig. 4. Coronal endorectal T2-weighted FSE image in a 30-year-old patient with primary infertility. The hyperintense cystic lesion in the dorsal midline of the prostate is compatible with a congenital cyst, associated with obstructed and markedly enlarged seminal vesicles bilaterally. The sperm count returned to normal following cyst incision under ultrasound guidance

Fig. 6 A, B. Preoperative work-up in a 70-year-old man with histologically confirmed prostate carcinoma. **A** Axial endorectal T2-weighted FSE image: The normally hyperintense seminal vesicle content is homogeneously decreased, compatible with tumor infiltration. **B** Congo Red stain (magnification × 100) of the seminal vesicles showing homogeneous red-brown subepithelial and intraluminal amorphous eosinophilic deposits which appear apple-green under polarized light, compatible with seminal vesicle amyloidosis. (From [16])

the peripheral zone as hyperintense and the "central gland", i.e., the central and transition zones, as hypointense (Fig. 1). The seminal vesicles are paired glands lying above the prostate. Their contents are homogeneous and hypointense (similar to muscle) on T1-weighted images and hyperintense on T2-weighted images. The vesicle walls enhance on gadolinium administration (Fig. 2).

The main indication for MRI in prostate disease is the pretreatment workup of carcinoma. In benign disease it is indicated only in isolated cases, but because benign conditions are a frequent incidental finding during the investigation of other prostate disease, radiologists need to be familiar with their features.

Benign disease of the prostate and seminal vesicles

Diagnosis of congenital prostate cysts has increased in parallel with the use of transrectal sonography and MRI in prostate diagnosis. The incidence of cysts is variously reported as 1–7.9 % [3, 4]. Their characteristic midline location makes them readily identifiable on MRI. They comprise utricular and Mullerian duct cysts. The two differ in embryonic origin: utricular cysts are more common and of endodermal origin [3, 5–7], whereas Mullerian duct cysts are of mesodermal origin. Further differentiating features are that utricular cysts often communicate with the prostatic urethra (best demonstrated on sagittal views) and may therefore contain spermatozoa, whereas Mullerian duct cysts (which tend to project cranially above the prostate) never communicate with the posterior urethra and often contain calcifications [3–9]. Utricular cysts can be associated with hypospadias, pseudohermaphrodism, cryptorchidism, and unilateral renal agenesis. For this reason, they are often diagnosed in childhood. The contents are hyperintense on T2-weighted images. Both types of cyst can cause symptoms such as dysuria, urinary tract infections, prostatitis, and infertility (Fig. 3) [3–9]. Smaller cysts are mostly incidental findings (Fig. 4).

Benign prostate hyperplasia impairs micturition in half of all men over 50 years. The conventional therapy is transurethral resection of the prostate (TURP), with open prostatectomy reserved for very large adenomas. Of American men over 60 years, 20–40 % are likely to require prostatectomy at current surgery rates [10, 11]. Benign prostate hyperplasia is not an indication for MRI but is a frequent incidental finding in patients investigated for other reasons, e.g., local staging of prostate carcinoma (Fig. 5).

Amyloid deposits in the seminal vesicles are a fairly common histologic finding in elderly subjects, with rates of 34 % at autopsy in those more than 75 years old people [12–15]. Senile amyloidosis can narrow the lumen and lower the normally hyperintense vesicle content signal on T2-weighted images, prompting a mistaken diagnosis of seminal vesicle infiltration [16–18]. Pathologic focal or diffuse lowering of signal intensity is observed in tumor infiltration by a prostate or vesicle carcinoma. Seminal vesicle infiltration can also be mimicked by hemorrhage (e.g., associated with biopsy or urogenital tract infection), a hypointense vas deferens, and a large vesicle-displacing adenoma, as well as amyloid [19]. Contrast-enhanced sequences may be helpful in distinguishing amyloidosis from tumor invasion. In amyloidosis, only the septa enhance, whereas in tumor invasion the content within the vesicles enhance as well. It might be difficult, however, to exclude early tumor invasion with focal thickening of septa, and in case of doubt, TRUS-guided biopsies of the seminal vesicles may be needed to establish the correct diagnosis (Fig. 6) [20, 21].

Prostate carcinoma

In industrialized countries prostate carcinoma is the most frequent cancer in men after carcinoma of the bronchus, and its incidence is increasing [22, 23]. The early stages are generally asymptomatic. Most cancers are therefore revealed by a raised prostate specific antigen (PSA) value or positive digital rectal examination, with biopsy confirmation. Grade is – next to tumor volume – one of the strongest predictors of biologic behavior in prostatic adenocarcinoma, including invasiveness and metastatic potential, but is not reliable when used alone in predicting pathologic stage or patient outcome for individual patients. Grade is included among other prognostic factors in therapeutic decision making, including patient age and health, accurate clinical stage, and serum PSA level. When stage of disease is factored in with grade, prognostication is enhanced. At the high end of the spectrum, with Gleason grade of 8–10, the incidence of lymph node metastases ranges between 20 and 61 % [24, 25].

Whereas bone scintigraphy with ^{99m}Tc-DPD has become the generally accepted method for excluding bone metastases, the investigation of choice for local tumor extension remains a matter of dispute. In localized prostate cancer (stages T1 and T2), life expectancy after radical prostatectomy (including the seminal vesicles) is similar to that in age-matched controls. However, in advanced local disease (T3/T4) benefit is questionable. Accurate pretreatment work-up is therefore critical in determining management. The task of imaging is to differentiate the T1 and T2 stages localized to the prostate from advanced tumor spread. Microcapsular invasion is an ambiguous area in this context. However, it appears not to worsen the prognosis provided the resection margins are free of tumor [26].

For this purpose the accuracy of endorectal MRI is approximately 80 % [27–37]. However, the Radiology Diagnostic Oncology Group study shows considerable interindividual differences in interpretation. Accuracy rates for experienced radiologists were 79 vs 54 % for less experienced colleagues [34]. Contrast-enhanced T1-weighted endorectal sequences in addition to T2-weighted images do not generally improve the results but may be valuable in isolated cases, e.g., if the image quality of the T2-weighted sequence is impaired by motion artifacts (Figs. 7–9) [29, 34, 38].

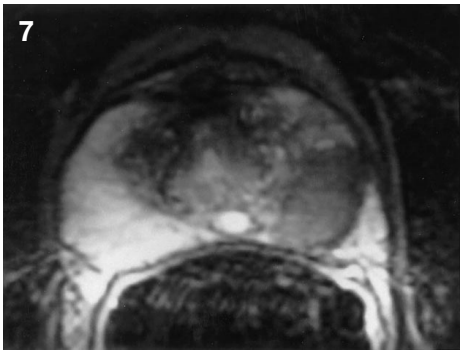

Fig. 7. Axial endorectal T2-weighted FSE image: The normally hyperintense peripheral zone of the prostate shows decreased signal intensity on the left side, compatible with infiltrating tumor. No evidence of capsule invasion. Histology: stage pT2 adenocarcinoma. Coincidental finding: small congenital prostate cyst

Fig. 8 A, B. Histologically confirmed prostate carcinoma stage pT3. **A** Axial endorectal T2-weighted FSE image: Tumor infiltration of the entire prostate gland and extension into the right neurovascular bundle *(arrow)*. **B** Axial endorectal T2-weighted FSE image: Hypointense tumor invades the normally hyperintense seminal vesicle *(arrows)*

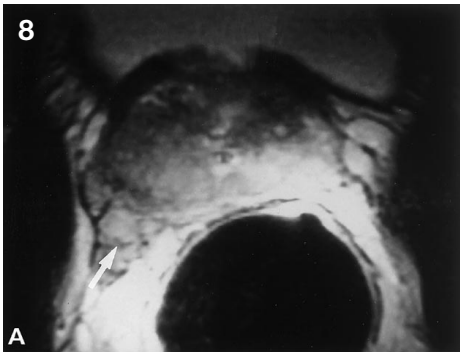

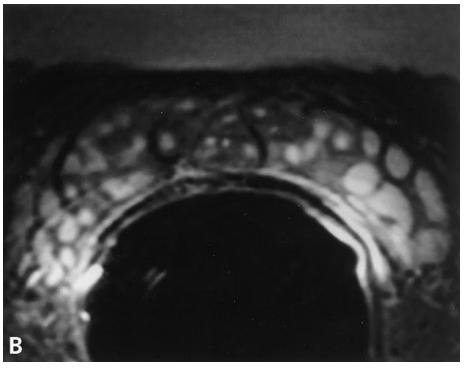

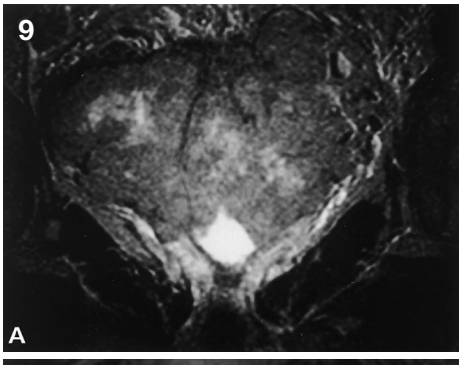

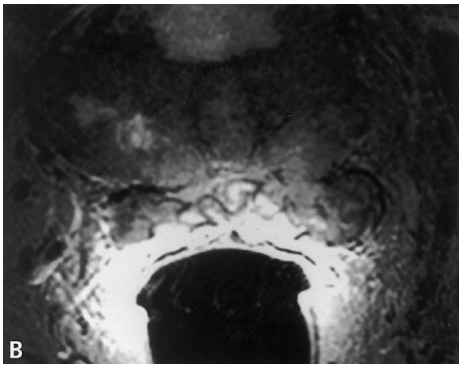

Fig. 9 A, B. Histologically confirmed high-grade prostate carcinoma stage pT4 in a patient with normal prostate specific antigen values. **A** Axial and **B** coronal endorectal T2-weighted FSE image: Tumor infiltration of the entire prostate gland with capsular penetration and invasion of the seminal vesicles (B) and urinary bladder

Fig. 10 A, B. Histologically confirmed recurrent prostate carcinoma. **A** Axial endorectal T2-weighted FSE image: Lobulated mass in the prostatic fossa of medium signal intensity *(arrow)*. **B** Axial endorectal contrast-enhanced T1-weighted image: The mass shows avid contrast-enhancement indicative of tumor recurrence rather than scar tissue *(arrow)*

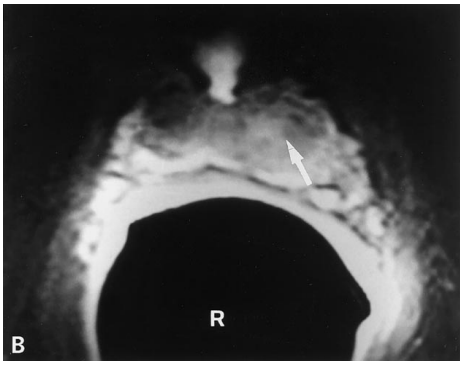

Lymph node metastases are a major determinant of prognosis and therapy in prostatic carcinoma [40]. Rates of lymph-borne metastasis depend on tumor volume, histologic differentiation, and stage [41]. Malignant lymph nodes tend either to exceed 1.5 cm in diameter or to be multiple. The literature on lymph node staging with both MRI and CT is disappointing with sensitivities of 50–60 %, no doubt due to the high amount of micrometastases in normal-sized nodes [41–45].

Locally recurrent prostate carcinoma

The frequency of local recurrence after radical prostatectomy is approximately 10 % [46]. If detected in its early stages by clinical examination and serial PSA [47], it can often be controlled by radiation or systemic therapy [47, 48]. Prostate specific antigen is a highly sensitive posttreatment tumor marker. However, it can be elevated in both local recurrence and distant metastasis [49]. Transrectal US is the imaging modality of choice for visualizing the prostatic bed. However, residual prostate

tissue is found anterior to the vesicourethral anastomosis in up to 80 % of patients. For this reason it can be difficult to differentiate between a small local recurrence, residual normal prostate tissue, and scar tissue, particularly given the postoperative changes in anatomical relationships [47, 48].

The advantage of MRI is high soft tissue contrast, enabling it to view the prostatic bed in each desired plane. Tissues can be differentiated by taking a global view of the data from the various sequences: on T2-weighted images residual prostate tissue is hyperintense, whereas local recurrence and scar tissue are hypointense. Contrast permits further differentiation: tumor tissue generally enhances, whereas scar tissue, except in the first 3–6 postoperative months, generally does not (Fig. 10) [50–53].

Endorectal MRI may therefore be a valuable backup to US. Body coil MRI can scan the regional lymph nodes and bony pelvis. However, this has only limited clinical significance because distant metastases are rare in this preselected group of patients with generally low PSA values and small tumor volume.

The scrotum

Although the scrotum is a superficial structure, its clinical examination frequently fails to provide a specific diagnosis because the clinical history and physical findings are similar under many conditions. Scrotal US, considered an extension of the physical examination, confirms the presumptive clinical diagnosis and provides relevant additional information. In most clinical problems, US supplies sufficient information for the correct diagnosis. Significant improvements in US were achieved with the introduction of color-coded duplex sonography (CCDS) and of power Doppler US, which provide information on blood flow over the entire area of the gray-scale image. A CCDS or power Doppler examination is indicated in any situation in which additional information on perfusion is needed to establish the diagnosis, particularly in testicular torsion, inflammation, scrotal trauma, and varicocele [54–56]. Other imaging modalities, except in the staging of testicular cancer, should be used only as problem-solving approaches. Besides US, MR imaging is a particularly useful modality. The latter is primarily used when the US findings are equivocal or suboptimal, or when there is a discrepancy between clinical and US findings.

Normal anatomy

Ultrasound depicts the normal (postpubescent) testicle as a fine-grained structure of homogeneous texture and medium echogenicity (Fig. 11), which is typically interrupted only by the hyperechoic mediastinum testis (Fig. 12). The latter shows wide interindividual variation in width and may also differ intraindividually between the right and left testis. The epididymis can best be differentiated from the testis on a longitudinal scan. Its thickest part is the head, which is visualized as a small cap-like structure situated on the upper pole of the testis. It may vary in shape and its diameter ranges from 5 to 12 mm. The body of the epididymis is a very delicate and flat structure with a diameter of approximately 2–4 mm and is thus not always delineated from adjacent tissue. The tail of the epididymis is also very flat (approximately 2–5 mm) and surrounds the lower testicular pole in a crescent-shaped manner. The testicular and epididymal appendages are usually too small to be always visualized on US scans. The testis and epididymis are surrounded by a cleft-like space, the so-called cavum serosum testis. This space may be filled with a small amount of fluid even under physiologic conditions and may thus be depicted as a thin anechoic margin (1–3 mm in width), typically around the epididymal head.

On MR imaging, the testes are homogeneous and isointense to muscle on T1-weighted images and higher in signal intensity on T2-weighted images [57]. The tunica albuginea is best seen as a low-intensity line on T2-weighted images; the mediastinum testis can also be identified as a low-intensity band. On T1-weighted images, the signal intensity of the epididymis is slightly heterogeneous and hypo- to isointense relative to the testis. The epididymis is more clearly differentiated from the testis on T2-weighted images because of its lower signal intensity compared with the adjacent testis. Intravenous administration of contrast material (e. g., Gd-DTPA) results in hyperintensity of the epididymis relative to the testis [58].

Fig. 11. Normal testis and epididymis. The testis has a homogeneous echo pattern and there is good differentiation between the testis and the head *(curved arrow)* and tail *(arrow)* of the epididymis ▶

Fig. 12 A, B. The mediastinum testis *(arrow)* is shown as a hyperechoic area. **A, B** It lies eccentrically in the testis, facing the epididymis. **B** The septa run toward the mediastinum testis and are typically not seen on ultrasound

Fig. 13 A–C. Seminoma of the left testicle. Longitudinal scan of **A** left testis and **B** transverse scan of both testes. Ultrasound demonstrates a hypoechoic intratesticular mass surrounded by a small rim of remaining testicular tissue. **C** Gross specimen. (From [33])

Fig. 14 A, B. Seminoma, with extensive, partly liquefied necrosis. **A** Transverse ultrasound demonstrates an enlarged testis with irregular, partly cystic alterations. Small amount of fluid around the testicle corresponding to a small hydrocele. **B** Gross specimen. (From [33])

Fig. 15 A–C. Malignant non-seminomatous germ cell tumor (embryonal carcinoma). **A** Axial endorectal contrast-enhanced T1-weighted image: The mass in the left testis *(arrow)* shows decreased contrast enhancement compared with the normal testicular tissue. **B** Axial endorectal T2-weighted FSE image of the testis: Well-defined isointense mass in the left testis *(arrow)*, hydrocele. **C** Hematoxylin and eosin stain (magnification × 50): undifferentiated epithelial-like tumor cells with high mitotic activity and pleomorphic nuclei

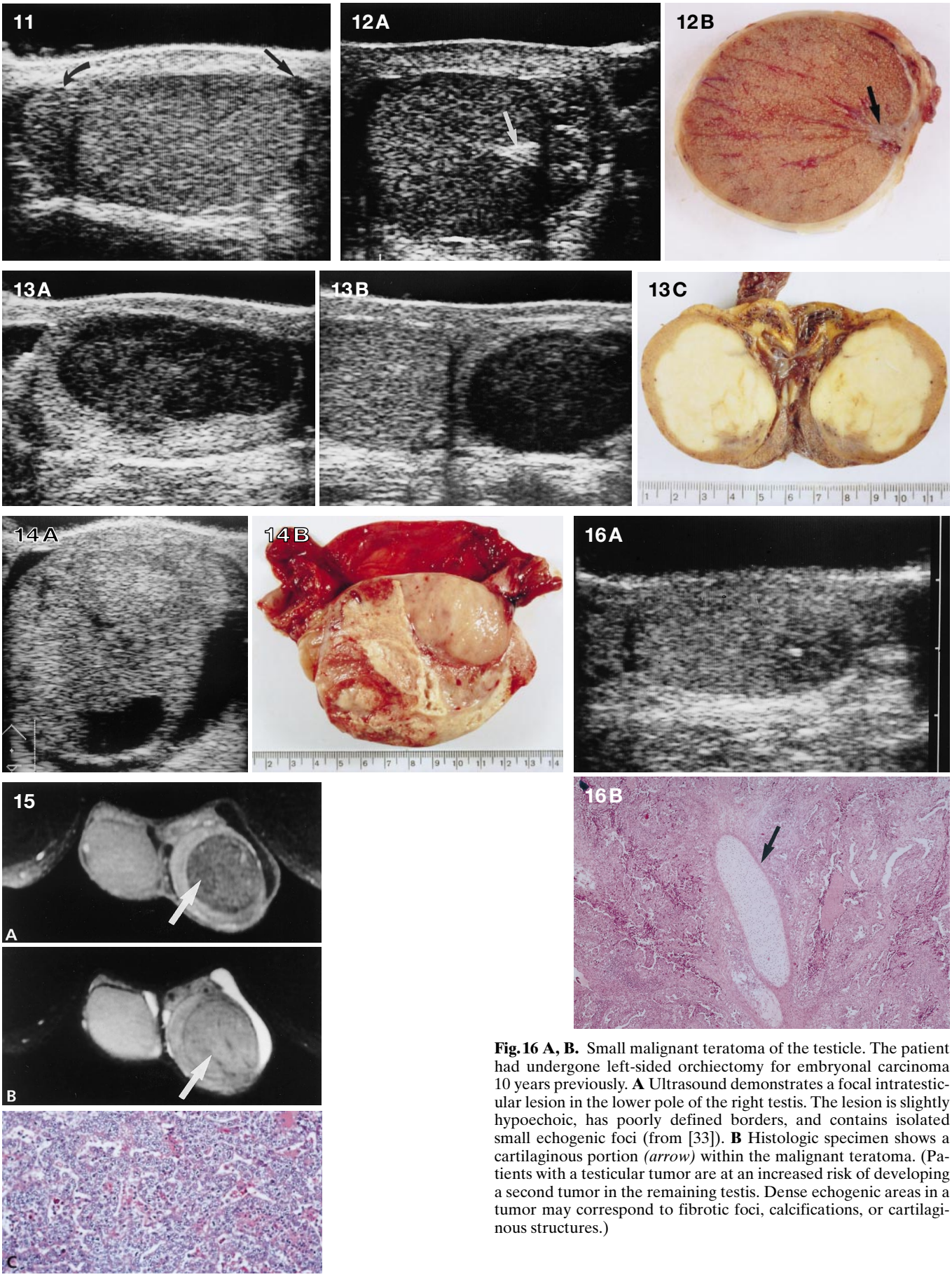

Fig. 16 A, B. Small malignant teratoma of the testicle. The patient had undergone left-sided orchiectomy for embryonal carcinoma 10 years previously. **A** Ultrasound demonstrates a focal intratesticular lesion in the lower pole of the right testis. The lesion is slightly hypoechoic, has poorly defined borders, and contains isolated small echogenic foci (from [33]). **B** Histologic specimen shows a cartilaginous portion *(arrow)* within the malignant teratoma. (Patients with a testicular tumor are at an increased risk of developing a second tumor in the remaining testis. Dense echogenic areas in a tumor may correspond to fibrotic foci, calcifications, or cartilaginous structures.)

Mass lesions

Malignant masses

Testicular cancer is the most common malignancy of the scrotum, whereas malignant tumors of the epididymis and of the spermatic cord are extremely rare. Cancer of the testis constitutes 1% of all malignancies in men; however, it is the most frequent cancer in the 15- to 34-year age group [59]. Testicular tumors comprise germ cell tumors, tumors originating in the gonadal stroma, tumors of the lymphoid and hematopoietic system, and secondary tumors (metastases). Germ cell tumors are by far the most frequent type (ca. 95%) [60, 61]. In addition, the testicles may be affected by tumor-like lesions.

Testicular cancer is typically noted as a lump or painless swelling of the testis. The presence of pain does not exclude testicular cancer; it is present in approximately 25% of cases.

The homogeneous parenchyma of the normal testis provides an excellent background for the depiction of intratesticular lesions by both US and MR imaging (Fig. 13). Small tumors are visualized as focal lesions, whereas larger ones may alter the entire testicular structure. The margins of testicular tumors may be smooth or irregular. On US, testicular tumors are typically hypoechogenic but may also be hyperechoic or of mixed echogenicity [62, 63]. Intratumoral necroses, hemorrhages, or cysts are depicted as liquid areas (Fig. 14). On MR imaging, testicular tumors most commonly show a signal intensity similar to that of the normal testis on T1-weighted images. On T2-weighted images, they are mostly hypointense relative to the normal testis with a homogeneous or heterogeneous signal pattern and only rarely demonstrate a signal intensity resembling that of healthy testicular tissue [64]. Color-coded duplex sonography depicts testicular tumors as areas of increased, reduced, or mixed perfusion, and thus does not add any information for lesion characterization [63]. The same also holds true for gadolinium-enhanced MR imaging (Fig. 15) [64, 65].

Seminomas typically have a hypoechoic and homogeneous texture on US (Fig. 13) and are of homogeneously low signal intensity on T2-weighted MR images [62, 64–66] Heterogenic areas within a seminoma are produced by regressive processes such as necrosis (Fig. 14).

Nonseminomatous tumors (e. g., embryonal carcinoma, choriocarcinoma, teratoma) are characterized by an inhomogeneous appearance [62, 67]. Marked heterogeneity in nonseminomatous tumors results from hemorrhage, fibrosis, calcification, or cartilage [62, 68]. Ultrasound depicts such structures (apart from hemorrhage) as dense echogenic foci (Fig. 16). Cystic spaces predominantly occur in teratomas [67]. Since these tumors frequently display a higher signal intensity on T2-weighted images, they may be isointense or slightly hyperintense relative to the normal testicular tissue. Therefore, an additional clinical examination is of particular importance for not missing such isointense testicular tumors.

Testicular intraepithelial neoplasia (TIN) is regarded as the common precursor of all germ cell tumors according to the uniform histogenesis theory [69]. This theory postulates that all germ cell tumors arise from identical precursor cells, namely testicular intraepithelial neoplasia. These changes at the cellular level, which may also be regarded as precancerous, cannot be identified by either US or MR imaging. In patients with unilateral testicular cancer, US can be used to check for a contralateral nonpalpable tumor. An irregular testicular tissue or coarse echogenic spots in these patients should give rise to the suspicion of a carcinoma in situ (CIS) [70].

Benign masses

Benign neoplasms of the testis account for only approximately 5% of all testicular neoplasms. They may arise from Leydig cells, Sertoli cells, or connective tissue stroma. These tumors typically have a homogeneous appearance and are smoothly demarcated. Neither US nor MR imaging can reliably distinguish these tumors from malignant neoplasms of the testis.

Epidermal cysts are tumor-like lesions of the testis. They are benign and filled with horny tissue. Enucleation of the lesion is required since only histology allows differentiation from teratoma. This intervention is presently performed with preservation of the remaining testicular tissue. On US some epidermal cysts actually resemble cysts in that they may show a markedly hyperechoic contour, but their distinctive feature is the presence of additional internal echoes and a posterior acoustic shadow (Fig. 17) [67].

Adenomatoid tumors are the most common extratesticular neoplasms. They most frequently arise in the epididymis but may also be found in the spermatic cord or tunica albuginea. Adenomatoid tumors are depicted as round lesions, typically demarcated by smooth borders. On US they are usually hyperechoic and homogeneous in appearance [71] but may also be hypoechoic or heterogeneous [72]. They are typically located in the tail of the epididymis (Fig. 18). Adenomatoid tumors may be difficult to distinguish from epididymal granuloma (or sperm granuloma). A history of previous inflammation, trauma, or surgery (vasectomy) helps to establish the diagnosis of epididymal granuloma.

Simple testicular cysts are rare, and reliable distinction of these benign cysts from malignant cystic tumors is of primary importance. The correct diagnosis can nearly always be made by palpation in combination with US (Fig. 19). Sonographically, cystic portions of malignant neoplasms are seen as multiple cysts disseminated within an inhomogeneous lesion, which is palpated as a firm mass. In contrast, a simple intratesticular cyst is never discovered as a palpable mass [67]. Instead, it is an incidental finding on US and is located close to the mediastinum testis. It is a solitary lesion in the majority of cases, but multiple lesions are also seen. Histologic examinations have shown that simple intratesticular cysts originate from the rete testis. Magnetic reso-

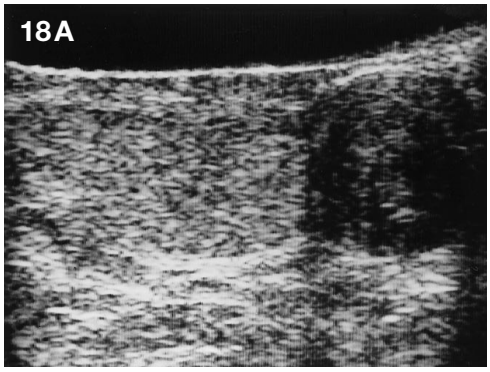

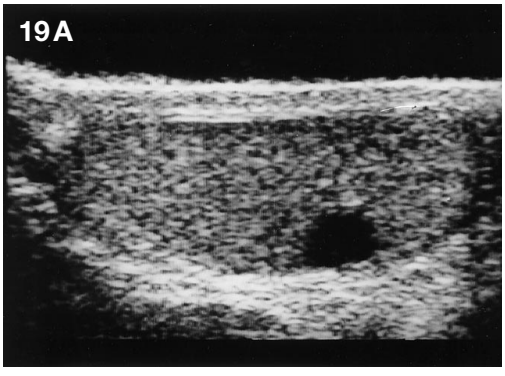

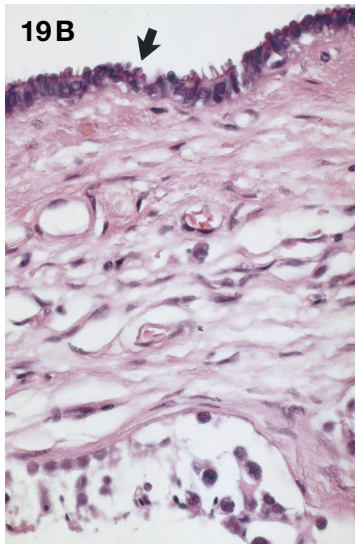

Fig. 17 A, B. Epidermoid cyst. **A** Ultrasound shows an intratesticular, echo-poor lesion with hyperechoic anterior and posterior margins. The lesion has a "cyst-like" appearance but contains internal echoes and shows posterior acoustic shadowing. **B** Gross specimen. (From [33])

Fig. 18 A, B. Adenomatoid tumor of the epididymis. **A** Solid, hypoechoic mass in the area of the tail of the epididymis. The tumorous lesion is clearly differentiated from the testis. **B** Surgical specimen, excised epididymis. (From [33])

Fig. 19 A, B. Simple testicular cyst. **A** Palpation findings were normal and the cyst was discovered only at ultrasound. The surrounding testicular parenchyma is of a homogeneous appearance. **B** Histologic specimen demonstrating a regular cystic wall lined with epithelium *(arrow)*

Fig. 20 A, B. Chronic inflammatory hydrocele secondary to recurrent epididymitis. **A** Thick-walled, septated hydrocele. The testicle *(arrow)* is small and deformed. **B** Surgical specimen

nance imaging typically depicts testicular cysts as sharply demarcated lesions showing the characteristic signal intensity of fluid. Their relationship to the mediastinum testis can easily be demonstrated.

Spermatoceles are common cysts of the epididymis. Their lumen is lined with an epithelial layer and is filled with fluid in which sediments of detritus, immobile spermatozoa, and lipids are identified. Clinically, spermatoceles manifest as palpable, moderately painful masses at the upper pole of the testis. Ultrasound and MR imaging clearly depict a cystic, smoothly demarcated lesion typically located in the epididymal head. Spermatoceles may be unilateral, bilateral, solitary, or multiple in location. In most cases, US reliably distinguishes spermatoceles from solid tumors. A spermatocele can, however, be associated with a dilatation of the rete testis and this condition may occasionally mimic a testicular tumor [73].

Hydroceles are pathologic fluid accumulations located between the two layers of the tunica vaginalis testis. They may be idiopathic in origin or develop in association with inflammation (epididymitis or orchitis), secondary to trauma or testicular torsion, and in the presence of a testicular tumor. Clinically, hydroceles are usually painless but frequently prevent palpation of the underlying testis. They are reliably diagnosed by US as an anechoic fluid collection with smoothly demarcated borders. Ultrasound thus yields a definitive diagnosis of a hydrocele and excludes underlying pathologic conditions of the testis or epididymis. Chronic hydroceles frequently develop septa and their wall becomes thickened. They may compress or deform the testicle (Fig. 20).

Magnetic resonance imaging is hardly ever indicated for diagnosing a hydrocele. On MR images, hydroceles show the characteristic features of fluid and typically represent an incidental finding.

Acute scrotum

The term "acute scrotum" comprises all disease entities that are characterized by the sudden onset of scrotal symptoms such as pain, swelling, and reddening. These symptoms may occur alone or in combination. From a clinical perspective, it is important to rapidly decide which patients presenting with an acute scrotum require immediate emergency surgery (e. g., testicular torsion or rupture) and which require initial drug treatment only (e. g., inflammation). Physical examination of the acute scrotum is limited by swelling and/or pain, therefore imaging may play a crucial role in identifying the cause of an acute scrotum. Color-coded duplex sonography has a central role in the differential diagnosis of an acute scrotum, since inflammatory processes are associated with hypervascularization, whereas testicular torsion is characterized by the absence of perfusion [56, 64].

Epididymitis and orchitis

Of all pathologic conditions affecting the epididymis, epididymitis is the most frequent cause of an acutely swollen and painful scrotum in adult men. Acute unspecific epididymitis is nearly always caused by descending, intracanalicular spread of pathogens in patients with prostatitis, urethritis, or other urinary tract infections. Concomitant orchitis is found in up to 20 % of patients with epididymitis. Isolated orchitis is rare except when caused by a viral infection such as mumps.

During the acute stage, the epididymis is markedly enlarged (Fig. 21) and, depending on the extent of the inflammatory process, swelling may affect either the entire organ or be confined to the tail. On clinical examination, the testis and epididymis usually cannot be palpated separately; however, differentiation should always be possible on US or MR imaging. An acutely inflamed epididymis usually has an inhomogeneous echo texture with a coarse distribution of echoes (Fig. 21). Compared with the normal testis, the echogenicity of the epididymis is typically reduced but may occasionally be increased (possibly because of epididymal hemorrhages) [74, 75]. On MR imaging, the affected epididymis is enlarged and demonstrates a heterogeneous, mostly high signal intensity on T2-weighted images. Acute epididymitis may be complicated by hemorrhages, producing varying signal intensities on T1- and T2-weighted images. T1-weighted images depict inflammatory infiltration and multiple engorged vessels with signal void due to hypervascularity. Inflammatory areas are markedly enhanced on gadolinium-enhanced T1-weighted images.

The diagnosis of epididymo-orchitis is suggested by the sonographic demonstration of an area of decreased echogenicity in the testis [64]. The involved area (typically in the upper pole of the testis) or even the entire organ most commonly demonstrates a homogeneous decrease in echogenicity. The hypervascularization associated with inflammation can most easily be demonstrated by CCDS, which thus has a key role in differentiating inflammation from testicular torsion (Fig. 21). In severe orchitis, the testis is hypoechoic and its echo texture becomes more heterogeneous, and early abscess formation may be overlooked. Therefore, such patients require sonographic follow-up, whereas patients with uncomplicated epididymitis do not. On T2-weighted MR images, testicular inflammation appears as a homogeneous or heterogeneous hyperintense lesion, which, unlike a testicular tumor, usually does not produce a mass effect. The testicular septula remain well defined but are thickened, a finding which is in contrast to the loss of normal architecture frequently observed with invasive neoplastic disease [57, 65]. Abscess formation may occur (Fig. 22).

Granulomatous orchitis poses a particular diagnostic problem both on US and on MR imaging. Fever and pain are often absent, and palpation may reveal a firm mass mimicking a testicular tumor. Sonographically, granulomatous orchitis is characterized by enlargement of the organ and an echopenic, inhomogeneous structure, which does not allow distinction from a testicular tumor. The same holds true for MR imaging.

Testicular torsion

The term "testicular torsion" denotes the rotation of the testis around the longitudinal axis of the spermatic cord (Fig. 23). It requires immediate emergency surgery to prevent irreversible damage to testicular tissue. Approximately 65 % of cases occur in young males (between 12 and 18 years of age). Too much emphasis, however, should not be put on age, since the three most frequent causes of an acute scrotum (epididymitis and torsion of a testicle or an appendage) occur in all age groups. Testicular torsion may occur in an otherwise completely healthy individual and manifests by a sudden onset of scrotal pain followed by swelling.

The sonographic appearance of testicular torsion is unspecific and diagnostic information from gray-scale

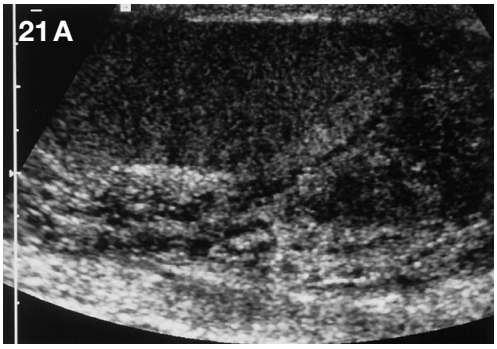

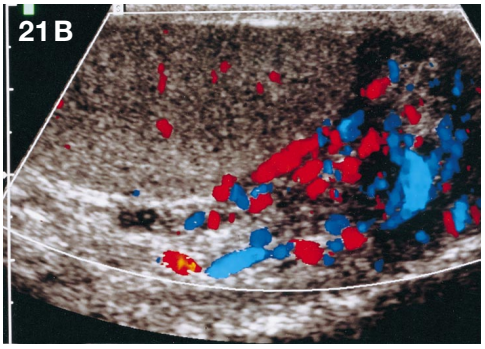

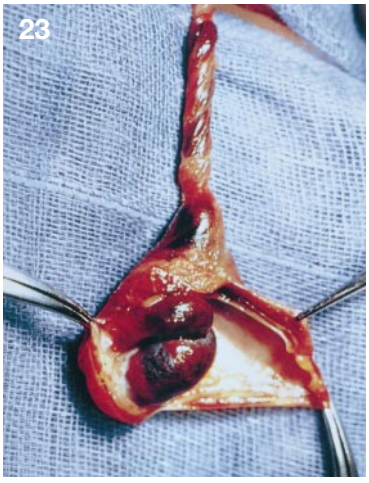

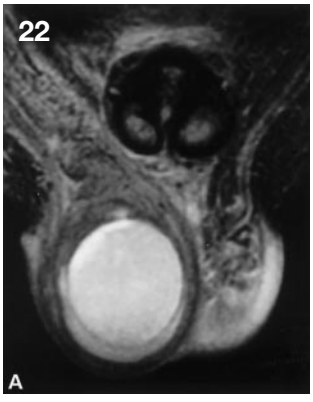

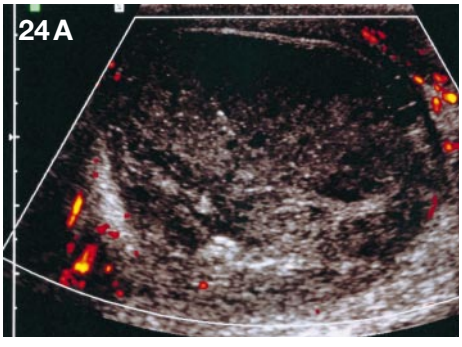

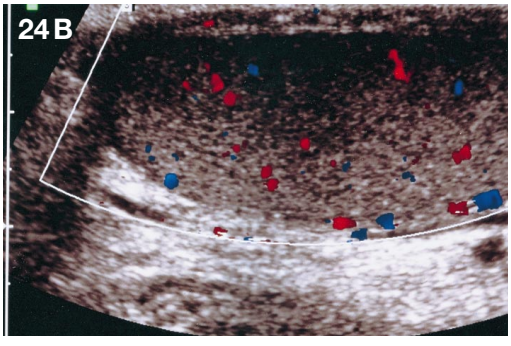

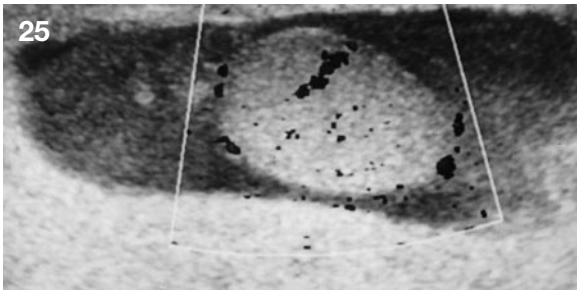

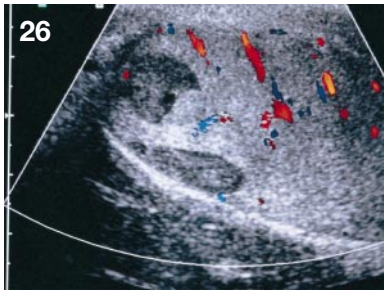

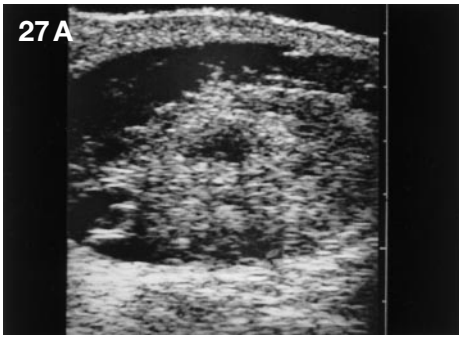

Fig. 21 A, B. Epididymitis. **A** Pronounced enlargement and inhomogeneity of the epididymis. **B** CCDS demonstrates an increased blood flow in the inflamed epididymis

Fig. 22 A, B. Testicular abscess formation. The abscess presents hyperintense on the coronal T2-weighted FSE and hypointense on the contrast-enhanced T1-weighted image of the testis. Inflammatory changes in the surrounding tissue

Fig. 23. Testicular torsion in a 4-day-old newborn with hemorrhagic necrosis of the testis and epididymis (intraoperative finding)

Fig. 24 A, B. Testicular torsion. **A** Power Doppler ultrasound demonstrates absence of blood flow from the enlarged and inhomogeneous testicle and epididymis; increased blood flow in the peritesticular tissue. **B** Regular intratesticular blood flow in a normal testicle on CCDS, shown for comparison

Fig. 25. Posttraumatic hematocele in a 10-year-old boy. The power Doppler mode shows normal perfusion of the testicle and thus excludes traumatic testicular torsion

Fig. 26. Posttraumatic intratesticular hematomas. The hematomas are depicted as hypoechoic areas. The testicular contour is preserved. The power Doppler mode shows normal testicular perfusion and thus excludes traumatic testicular torsion

Fig. 27 A, B. Traumatic testicular rupture. **A** Ultrasound shows an irregular testicular contour with hypoechoic, ill-defined intratesticular areas and an accompanying hematocele. **B** Surgical specimen. (From [33])

US is limited [56, 76–78]. Therefore, US examination of the scrotum should include CCDS studies. No changes in intrascrotal structures are seen on gray-scale US at early stages of testicular torsion. Ultrasound depicts only changes resulting from hemorrhagic infarction at later stages – when it is too late in most instances for surgical correction [76]. With the advent of CCDS, it has now become possible to identify testicular torsion at an early stage [56, 80–83]. Whereas the normal testis and epididymis are characterized by the depiction of isolated flow signals, flow signals are significantly diminished in partial torsion and absent in complete torsion (Fig. 24). However, reactive hyperemia of the scrotal skin can be seen. It is important to bear in mind that the demonstration of blood flow in the testis does not exclude the possibility of partial torsion. In general, the reduction of blood flow to the testis is not immediate or complete; instead, there is a gradual decrease as the edema increases. Therefore, not only is the absence of blood flow an important diagnostic finding, but also a decrease compared with the normal contralateral side. Overall, CCDS has a sensitivity range from 82 to 90 %, whereas its specificity in diagnosing testicular torsion reaches 100 % [84].

Magnetic resonance imaging is only rarely performed in patients with suspected testicular torsion, not least of all due to the long examination times and logistic problems. Findings on MR imaging include an enlarged spermatic cord with diminished flow, diffusely decreased signal intensity of the testis, and mild to moderate thickening of the tunica albuginea and epididymis [84]. A twisted cord can be seen as multiple low-intensity curvilinear structures radiating in a "whirlpool" pattern, which is best depicted in a plane perpendicular to its axis. The point of the twist may be identified as an area of signal void (torsion knot). High-signal-intensity areas on T1-weighted images indicate diffuse intraparenchymal hemorrhage of the testis or epididymis.

Trauma

In patients with traumatic injuries to the testis, hematoma, hematocele, and intratesticular bleeding, or testicular rupture, have to be distinguished. Palpation is extremely restricted by severe pain and pronounced swelling.

Ultrasound easily depicts a soft tissue hematoma as an echopenic lesion and additional CCDS can exclude traumatic testicular torsion (Figs. 25, 26). The diagnosis of a hematocele is established by the sonographic demonstration of a "hydrocele-like" fluid accumulation which contains numerous small internal echoes (Fig. 27). On MR imaging, most hematoceles initially exhibit medium signal intensity on T1-weighted images and high signal intensity on T2-weighted images [57, 65]. Chronic hematoceles usually demonstrate high signal intensity on both T1- and T2-weighted images.

Intratesticular hemorrhages are depicted as lesions of low echogenicity on US, mostly with sharply demarcated borders and occasionally with a heterogeneous appearance (Fig. 26). A small tear in the tunica albuginea may be overlooked on US, but advanced testicular rupture is always visualized; the latter is associated with irregularities of the testicular contour and either hypo- or hyperechoic heterogeneous areas in the organ (Fig. 27). On MR imaging, the diagnosis of testicular rupture is facilitated by the excellent depiction of the tunica albuginea. The integrity of the tunica albuginea is best judged on T2-weighted or contrast-enhanced T1-weighted images. However, multiple planes of imaging are often needed for thorough evaluation. On T2-weighted images, the signal intensity of the injured testis is *lower* than that of the normal contralateral testis [65]. On contrast-enhanced T1-weighted images, the injured testis demonstrates less-pronounced enhancement. The signal intensity of intratesticular hematoma depends on the time interval elapsed between bleeding and MR imaging. In the acute phase, low or medium signal intensity is seen on T1-weighted images and high signal intensity on T2-weighted images. In the chronic phase, high signal intensity occurs on both T1- and T2-weighted images [85].

References

1. Hricak H, White S, Vigneron D et al. (1994) Carcinoma of the prostate gland: MR imaging with pelvic phased-array coils versus integrated endorectal-pelvic phased-array coils. Radiology 1193: 703–709
2. Kirby RS, Christmas TJ, Brawer M (1998) Prostate cancer: anatomical and pathological considerations. Mosby, Times Mirror International Publishers, St. Louis, pp 2–21
3. Dik P, Lock TMWT, Schrier BP, Zeijlemaker BYW, Boon TA (1996) Transurethral marsupialization of a medial prostatic cyst in patients with prostatitis-like symptoms. J Urol 155: 1301–1304
4. Mayersak JS, Kuchenbecker DA (1993) Mullerian duct cyst. Uroradiology 41: 176–180
5. McDermott VG, Meakem TJ III, Stolpen AH, Schnall MD (1995) Prostatic and periprostatic cysts: findings on MR imaging. AJR 64: 123–127
6. Schwartz JM, Bosniak BA, Hulnick DA, Megibow AJ, Raghavendra BN (1998) Computed tomography of midline cysts of the prostate. J Comput Assist Tomogr 12: 215–218
7. Gevenois PA, Van Sinoy ML, Sintzoff SA Jr, Stallenberg B, Salmon I, Van Regemorter G, Struyven J (1990) Cysts of the prostate and seminal vesicles: MR imaging findings in 11 cases. AJR 155: 1021–1024
8. Thurnher S, Hricak H, Tanagho E (1988) Mullerian duct cyst: diagnosis with MR imaging. Radiology 168: 25–28
9. Wachsberg RH, Sebastiano L, Sullivan BC, Irwin R (1995) Posterior urethral diverticulum presenting as a midline prostatic cyst: sonographic and MRI appearance. Abdom Imaging 20: 70–71
10. Barry MJ (1990) Epidemiology and natural history of benign prostatic hyperplasia. Urol Clin North Am 17: 495–507
11. Doll HA, Black NA, McPherson K, Flood AB, Williams GB, Smith JC (1992) Mortality, morbidity and complications following transurethral resection of the prostate for benign prostatic hypertrophy. J Urol 147: 1566–1573
12. Bursell S (1942) Beitrag zur Kenntnis der Paraamyloidose im urogenitalen Trakt unter besonderer Berücksichtigung der sogenannten senilen Amyloidose in den Samenbläschen und ihres Verhältnis zum Samenblasenpigment. Uppsala Läkaref Förh 47: 313–331

13. Fujihara S, Glenner GG (1981) Primary localized amyloidosis of the genitourinary tract: immunhistochemical study on eleven cases. Lab Invest 44: 55–60
14. Goldman H (1963) Amyloidosis of the seminal vesicles and vas deferens: primary localized cases. Arch Pathol 75: 94–98
15. Pitkanen P, Westermark P, Cornwell GG, Murdoch W (1983) Amyloid of the seminal vesicles: a distinctive and common localized form of senile amyloidosis. Am J Pathol 110: 64–69
16. Hutter B, Huch Böni RA, Hawelski S, Maurer R, Krestin GP (1995) Durch Amyloidose vorgetäuschte Tumorinfiltration der Samenblasen. RöFö Fortschr Röntgenstr 163: 184–185
17. Yasushi K, Sugimura K, Nagaoka S, Ishida T (1992) Amyloid deposition in seminal vesicles mimicking tumor invasion from bladder cancer: MR findings. J Comput Assist Tomogr 16: 989–991
18. Ramschandi P, Schnall MD, LiVolsi VA, Tomaszewski JE, Pollack HM (1993) Senile amyloidosis of the seminal vesicles mimicking metastatic spread of prostatic carcinoma on MRI. AJR 161: 99–100
19. Mirowitz S (1995) Seminal vesicles: biopsy related hemorrhage simulating tumor invasion at endorectal MR imaging. Radiology 185: 373–376
20. Schnall MD, Imai Y, Tomazewski J, Pollack HM, Lenkinski RE, Kressel HY (1991) Prostate cancer: local staging with endorectal surface coil MR imaging. Radiology 178: 797–802
21. Terris MK, McNeal JE, Freiha FS, Stamey TA (1993) Efficacy of transrectal ultrasound-guided seminal vesicle biopsies in the detection of seminal vesicle invasion by prostate cancer. J Urol 149: 1035–1039
22. American Cancer Society (1994) Cancer, facts and figures. American Cancer Society, Atlanta
23. Levi F, La Vecchia C, Lucchini F, Boyle P (1993) Cancer incidence and mortality in Europe, 1984–1987. Soz Präventivmed (Suppl 3) S155–-S229
24. Epstein JI, Pizor G, Walsh PC (1993) Correlation of logic findings with progression following radical retropubic prostatectomy. Cancer 71: 3582–3593
25. Oesterling JE, Brendler CB, Epstein JI et al. (1987) Correlation of clinical stage, serum prostatic acid, phosphatase and preoperative Gleason grade with final pathological stage in 275 patients with clinically localized adenocarcinoma of the prostate. U Urol 128: 92–98
26. Carter H, Coffey D (1988) Prostate cancer: the magnitude of the problem in the United States. In: Coffey DS, Resnick MI, Dorr FA, Karr JP (eds) A multidisciplinary analysis of controversies in the management of prostate cancer. Plenum Press, New York, pp 1–75
27. Huch Böni RA, Boner JA, Debatin JF, Trinkler F, Knönagel H, Hochstetter A von, Helfenstein U, Krestin GP (1995) Optimization of prostate carcinoma staging: comparison of imaging and clinical strategies. Clin Radiol 50: 593–600
28. Huch Böni RA, Hutter B, Trinkler F, Jochum W, Pestalozzi D, Krestin GP (1996) Präoperatives T-Staging des Prostatakarzinoms: Vergleich der endorektalen MRT mit bildgebenden und klinischen Methoden. Fortschr Röntgenstr 165: 152–158
29. Chelsky M, Schnall M, Seidmon E, Pollack H (1993) Use of endorectal surface coil magnetic resonance imaging for local staging of prostate cancer. J Urol 150: 391–395
30. Hricak H, White S, Vigneron D et al. (1994) Carcinoma of the prostate gland: MR imaging with pelvic phased-array coils versus integrated endorectal-pelvic phased-array coils. Radiology 193: 703–709
31. Nicolas V, Beese M, Keulers A, Bressel M, Kastendieck H, Huland H (1993) MR-Tomographie des Prostatakarzinoms – Vergleich konventionelle und endorektale MRT. Fortschr Röntgenstr 161: 319–326
32. Schiebler M, Schnall M, Pollack H et al. (1993) Current role of MR imaging in the staging of adenocarcinoma of the prostate. Radiology 189: 339–352
33. Tempany N, Zhou X, Zerhouni E et al. (1994) Staging of prostate cancer: results of Radiology Diagnostic Oncology Group project comparison of three MR imaging techniques. Radiology 192: 47–54
34. Quinn S, Franzini D, Demlow T et al. (1994) MR imaging of prostate cancer with an endorectal surface coil technique: correlation with whole-mount specimens. Radiology 190: 323–327
35. Cornud F, Belin X, Flam T et al. (1996) Local staging of prostate cancer by endorectal MRI using fast spin-echo sequences: prospective correlation with pathological findings after radical prostatectomy. Br J Urol 77: 843–850
36. Jager G, Ruijter E, Kaa CVD et al. (1996) Local staging of prostate cancer with endorectal MR imaging: correlation with histopathology AJR 166: 845–852
37. Yu K, Hricak H, Alagappan R, Chernoff D, Bachetti P, Zaudek C (1997) Detection of extracapsular extension of prostate carcinoma with endorectal and phased-array coil MR imaging: multivariate feature analysis. Radiology 202: 697–702
38. Huch Böni RA, Boner JA, Lütolf UM, Trinkler F, Pestalozzi D, Krestin GP (1995) Contrast-enhanced, endorectal coil MR imaging in local staging of prostate carcinoma. J Comput Assist Tomogr 19: 232–237
39. Mirowitz S, Brown J, Heiken J (1993) Evaluation of the prostate and prostatic carcinoma with gadolinium-enhanced endorectal coil MR imaging. Radiology 186: 153–157
40. Gervasi LA, Mata J, Easley JD, Wilbanks H, Seale C, Hawkins H, Calron CE, Scardino PT (1989) Prognostic significance of lymph node metastases in prostatic cancer. J Urol 142: 332–336
41. Kastendieck H, Bressel M, Henke A, Hüsselmann H (1980) Häufigkeit regionärer Lymphknotenmetastasen beim operablen Prostatakarzinom Dtsch Med Wschr 105: 1348–1354
42. Nicolas V, Beese M, Keulers A, Bressel M, Kastendieck H, Huland H (1994) MR-Tomographie des Prostatakarzinoms – Vergleich konventionelle und endorektale MRT. Fortschr Röntgenstr 161: 319–326
43. McLaughlin A, Ill P, Salzstein SL, McCullough DL, Gittes RF (1996) Prostatic carcinoma: incidence and location of unsuspected lymphatic metastases. J Urol 115: 89–94
44. Levine MS, Arger PH, Coleman BG, Mulhern CB, Pollack HM, Wein AJ (1981) Detecting lymphatic metastases from prostatic carcinoma: superiority of CT. AJR 137: 207–211
45. Jager GJ, Barentsz JO, Oosterhof GO, Witjes JA, Ruijs SJH (1996) Pelvic adenopathy in prostatic and urinary bladder carcinoma: MR imaging with a three-dimensional T1-weighted magnetization-prepared-rapid gradient-echo sequence. AJR 167: 1503–1507
46. Robey EL, Schellhammer PF (1987) Local failure after definitive therapy for prostatic cancer. J Urol 137: 613–619
47. Wassermann NF, Kapoor DA, Hildebrandt WC et al. (1992) Transrectal ultrasound in evaluation of patients after radical prostatectomy. Part I. Normal postoperative anatomy. Radiology 185: 361–366
48. Wassermann NF, Kapoor DA, Hildebrandt WC et al. (1992) Ultrasound in evaluation of patients after radical prostatectomy. Part II. Transrectal US and biopsy findings in the presence of residual and early recurrent prostatic cancer. Radiology 185: 367–372
49. Lange PH, Ercole CH, Lightner EJ et al. (1989) The value of serum prostate specific antigen determinations before and after radical prostatectomy. J Urol 141: 873–879
50. Ebner F, Ranner G, Flückiger F (1994) Differenzierung von Narbengewebe und Tumorrezidiv nach Therapie von Tumoren des weiblichen Beckens. Radiologe 34: 384–389
51. Schiebler M, Schnall M, Pollack H et al. (1993) Current role of MR imaging in the staging of adenocarcinoma of the prostate. Radiology 189: 339–352
52. Quinn S, Franzini D, Demlow T et al. (1994) MR imaging of prostate cancer with an endorectal surface coil technique: correlation with whole-mount specimens. Radiology 190: 323–327
53. Huch Böni RA, Meyenberger C, Pok Lundquist J, Trinkler F, Lütolf U, Krestin GP (1996) Value of endorectal coil versus

body coil MRI for diagnosis of recurrent pelvic malignancies. Abdom Imaging 21: 345–352
54. Fobbe F, Heidt P, Hamm B, Koennecke HC, Hauck G, Dieckmann KP, Wolf KJ (1989) Improved diagnosis of scrotal disorders by color-coded duplex sonography. Fortschr Röntgenstr 150: 629–634
55. Mitchell DG (1990) Color Doppler imaging: principles, limitations, and artifacts. Radiology 177: 1–10
56. Herbener TE (1996) Ultrasound in the assessment of the acute scrotum. J Clin Ultrasound 24: 405–421
57. Noone TC, Huch-Böni RA, Semelka RC (1997) Male pelvis. In: Semelka RC, Ascher SM, Reinhold C (eds) MRI of the abdomen and pelvis. Wiley-Liss, New York, pp 541–569
58. Müller-Leisse C, Bohndorf K, Stargardt A et al. (1994) Gadolinium-enhanced T1-weighted imaging of scrotal disorders: Is there an indication for MR imaging? J Magn Reson Imaging 4: 389–395
59. Silverberg E (1982) Cancer in young adults (ages 15–34). Cancer 32: 32–42
60. Mostofi FK (1973) Proceedings: testicular tumors, epidemiologic, etiologic, and pathologic features. Cancer 32: 1186–1201
61. Skakkebaek NE, Berthelsen JG, Giwercman A, Müller J (1987) Carcinoma in situ of the testis: possible origin from gonocytes and precursor of all types of germ-cell tumours except spermatocytoma. Int J Androl 10: 19–28
62. Schwerk WB, Schwerk WN, Rodeck G (1987) Testicular tumors: prospective analysis of real-time US patterns and abdominal staging. Radiology 164: 369–374
63. Hamm B (1997)Differential diagnosis of scrotal masses by ultrasound. Eur Radiol 7: 668–679
64. Hricak H, Hamm B, Kim B (1995) Imaging of the scrotum. Raven Press, New York
65. Cramer BM, Schiegel E, Thuroff J (1991) MR imaging in the differential diagnosis of scrotal and testicular disease. Radiographics 11: 9–21
66. Johnson JO, Mattrey RF, Philipson J (1990) Differentiation of seminomatous from nonseminomatous testicular tumors with MR imaging. Am J Roentgenol 154: 539–543
67. Hamm B (1994) Sonography of the testis and epididymis. Andrologia 26: 193–210
68. Grantham JG, Charboneau JW, James EM, Kirschling RJ, Kvols LK, Segura JW, Wold LE (1985) Testicular neoplasms: 29 tumors studied by high-resolution US. Radiology 157: 775–780
69. Skakkebaek NE, Berthelsen JG, Giwercman A, Müller J (1987) Carcinoma in situ of the testis: possible origin from gonocytes and precursor of all types of germ-cell tumours except spermatocytoma. Int J Androl 10: 19–28
70. Lenz S, Skakkebaek NE, Hertel NT (1996) Abnormal ultrasonic pattern in contralateral testes in patients with unilateral testicular cancer. World J Urol 14: S55–S58
71. Leonhardt WC, Gooding GA (1992) Sonography of intrascrotal adenomatoid tumor. Urology 39: 90–92
72. Frates MC, Benson CB, DiSalvo DN, Brown DL, Laing FC, Doubilet PM (1997) Solid extratesticular masses evaluated with sonography: pathologic correlation. Radiology 204: 43–46
73. Older R, Watson L (1994) Tubular extasia of the rete testis: a benign condition with a sonographic appearance that may be misinterpreted as malignant. J Urol 152: 477–478
74. Benson CB, Doubilet PM, Richie JP (1989) Sonography of the male genital tract. AJR 153: 705–713
75. Rifkin MD (1987) Scrotal ultrasound. Urol Radiol 9: 119–126
76. Middleton WD, Middleton MA, Dierks M, Keetch D, Dierks S (1997) Sonographic prediction of viability in testicular torsion: preliminary observations. J Ultrasound Med 16: 23–27
77. Hricak H, Jeffrey RB (1983) Sonography of acute scrotal abnormalities. Radiol Clin North Am 21: 595–603
78. Martin B, Conte J (1987) Ultrasonography of the acute scrotum. J Clin Ultrasound 15: 37–44
79. Stoller ML, Kogan BA, Hricak H (1985) Spermatic cord torsion: diagnostic limitations. Pediatrics 76: 929–933
80. Kass EJ, Stone KT, Cacciarelli AA, Mitchell B (1993) Do all children with an acute scrotum require exploration? J Urol 150: 667–669
81. Erden MI, Ozbek SS, Aytac SK, Adsan O, Suzer O, Safak SM (1993) Color Doppler imaging in acute scrotal disorders. Urol Int 50: 39–42
82. Fitzgerald SW, Erickson S, Wire DM de et al. (1992) Color Doppler sonography in the evaluation of the adult acute scrotum. J Ultrasound Med 11: 543–548
83. Wilbert DM, Schaerfe CW, Stern WD, Strohmaier WL, Bichler KH (1993) Evaluation of the acute scrotum by color-coded Doppler ultrasonography. J Urol 149: 1475–1477
84. Trambert MA, Mattrey RF, Levine D, Berthoty DP (1990) Subacute scrotal pain: evaluation of torsion versus epididymitis with MR imaging. Radiology 175: 53–56
85. Hamm B (1991) Sonographische Diagnostik des Skrotalinhalts – Lehrbuch und Atlas. Springer, Berlin Heidelberg New York

Book review

European Radiology

Strunk H., Gutjahr P.: Tumoren bei Kindern. Moderne Bildgebung mit MRT und CT. Vol. 2. Körperstamm und Extremitäten. Stuttgart, New York: Thieme 1996, 192 pages, 207 figures, 25 tables, ISBN 3-13-102981-1, DM 198.00

The series "Tumoren bei Kindern" is conceived as an atlas with text and pictures about diagnostic, therapy concepts and the course of the illness. This volume demonstrates the spectrum of tumors of the body and extremities.

There are 72 cases featured. Each one is dealt with in the same way: anamnesis, clinical findings and diagnostic imaging – CT and/or MRI – lead to the diagnosis; the differential diagnosis is shown; the therapy concept and the course is explained; finally, the case is discussed in an important commentary at the end.

Preceding these cases, there is a general section with a concise text about epidemiology, clinical findings, examination technique and preparation for CT and MRI, indication, therapy, diagnosis in the course of illness and prognosis, followed by an up-to-date bibliography.

The various tumors are discussed in the same way before the cases to which they refer; the tables give clear information about the possible tumors, e. g. neuroblastoma and nephroblastoma, and provide an overview of the stages. There is also an up-to-date-bibliography at the end.

The emphasis in this atlas is on imaging by MRI and/or CT. The diagnostic potential of MRI and CT is clearly shown. The concise text and the quality of the pictures are very impressive. More cases of tumors of the skeleton and soft tissue would be desirable. The atlas is not meant as a text book but is an aid to the interpretation of findings for everyone who deals with tumors of the body and extremities in children. The price is appropriate for this very informative book.

G. Benz-Bohm, Köln